Journal of Combinatorial Mathematics
and Combinatorial Computing
www.combinatorialpress.com/jcmcc

Construction of a Dynamic Early Warning Model for Cyanobacterial Blooms in Lake Taihu Combining Long-Time-Series Satellite Remote Sensing Data and Computational Intelligence

Yuzhuo Li[1,2,3,✉]

[1] *Key Laboratory of Digital Earth Science, Aerospace Information Research Institute, Chinese Academy of Sciences, Beijing, 100094, China*
[2] *International Research Center of Big Data for Sustainable Development Goals, Beijing, 100094, China*
[3] *University of Chinese Academy of Sciences, Beijing, 100049, China*

ABSTRACT

Frequent outbreaks of cyanobacterial blooms in Lake Taihu are undoubtedly a great threat to the economic development of its neighboring areas and the safety of drinking water of its residents. This paper takes Taihu Lake as the study area and analyzes its geographic location information and development status. Then, based on the remote sensing data from MODIS and Landsat 8 satellites, the normalized vegetation index is improved to identify the blooms, and the dynamic detection method of cyanobacterial blooms is constructed by combining with the remote sensing inversion of water temperature. At the same time, the spectral performance of each band is integrated to excavate the characteristic information of cyanobacterial bloom, and the algorithm in this paper is used to process the satellite remote sensing data of cyanobacterial bloom in Lake Taihu to analyze its spatial and temporal distribution characteristics, which is used as the basis of the dynamic warning model for early warning. Then the LightGBM method is introduced to realize the all-weather spatial and temporal continuous monitoring of cyanobacterial blooms in Lake Tai. Analyzing the monitoring data of this paper's model on the intraday change process of cyanobacterial bloom in Lake Taihu, it is found that the trend of intraday change in the area of cyanobacterial bloom in Lake Taihu in different seasons is relatively consistent, with the highest area of the bloom in autumn, accounting for 21% of the area of Lake Taihu's water body. The study pointed out that after entering the fall, extra attention should be paid to the monitoring, prevention and control of cyanobacterial bloom in Lake Taihu.

Keywords: Lake Taihu cyanobacterial bloom, LightGBM method, remote sensing technology, normalized vegetation index (NVI)

✉ Corresponding author.
E-mail address: bjlyz666@163.com (Y. Li).
Received 15 September 2024; Revised 05 November 2024; Accepted 20 February 2025; Published Online 16 April 2025.
DOI: 10.61091/jcmcc127b-151

1. Introduction

Taihu Lake is the second largest freshwater lake in China, with a mild climate and rich specialties in its basin, which has been famous as the land of fish and rice since ancient times. Lake Taihu is a famous tourist attraction in Jiangsu Province because of its beautiful and fascinating scenery [1-2]. However, with the increasing human activities, the Taihu Lake area is facing serious water environment problems, and the recent summer outbreaks of cyanobacteria almost every year have cast a shadow over the lake, bringing great challenges to water resources management and environmental protection [3-6].

The cyanobacterial outbreak in Taihu Lake is often referred to as eutrophication of water bodies, commonly known as water bloom, which is a natural phenomenon that occurs in freshwater and is caused by the high nitrogen and phosphorus content of water bodies, resulting in the sudden overproliferation of algae, and also a kind of secondary pollution, which usually presents a green or blue color of water [7-10]. Generally speaking, “bloom” is a natural ecological phenomenon in freshwater, involving cyanobacteria (i.e., cyanobacteria), green algae, diatoms and so on. The naturally occurring bloom phenomenon will disappear quickly and will not bring environmental impacts [11-14]. However, the frequent outbreaks of blooms in Taihu Lake, Dianchi Lake, Chaohu Lake, Hongze Lake and other places in China are inseparable from human factors, and humans yearn for the discharge of nitrogen (mainly ammonium, nitrate, and nitrite) and phosphorus (mainly orthophosphate and various forms of phosphate) in water bodies, resulting in eutrophication of freshwater, exceeding the environmental capacity and self-purification capacity, resulting in frequent "blooms", which spread year by year and extend their duration year by year [15-18].

Literature [19] combined field observation and satellite remote sensing data to analyze the influencing factors of the intensity of Lake Tai Lake cyanobacterial bloom during several years, and described the changes in the composition of phytoplankton community, climate, and water quality, and revealed that the temperature and permanganate index were the important parameters affecting the structure of phytoplankton community. Literature [20] determined that the water level of Lake Taihu was the influencing factor of cyanobacterial bloom by analyzing the correlation analysis of nitrogen, phosphorus, potassium and the area of cyanobacteria, and constructed the hazard function of cyanobacterial bloom in Lake Taihu, evaluated the economic loss caused by cyanobacterial bloom, and provided the basis for the control and management of cyanobacteria in Lake Taihu. Literature [21] proposed an upgraded framework for monitoring and predicting harmful cyanobacterial blooms, constructed a collaborative monitoring network for cyanobacterial blooms, realized the prediction of cyanobacteria in the whole lake and near-shore area, and revealed that the application of the framework in Chaohu Lake significantly improved the accuracy of monitoring and early warning of cyanobacterial blooms. Literature [22] monitored the spatial and temporal distribution of cyanobacterial blooms in Lake Taihu using Landsat images from a cloud computing platform and calculated the percentage of the area of cyanobacterial blooms and the frequency index of cyanobacterial blooms, indicating that cyanobacterial blooms in Lake Taihu diffused from the north to the central, western and eastern parts of the lake. Literature [23] designed a cyanobacteria prediction model for Lake Taihu based on machine learning, evaluated the regional and temporal characteristics of the daily changes of the bloom on an hourly scale, and revealed that the meteorological conditions could affect the occurrence of cyanobacterial bloom on multiple time scales, which verified the effectiveness of the model. Literature [24] proposed a fine range of continuously varying response thresholds to characterize the relationship between Chla concentration and NH4-N, total nitrogen (TN) and total phosphorus (TP) concentrations, pointing out that TP is the dominant factor affecting the spatial variation of cyanobacterial blooms in most areas of Lake Taihu. Literature [25] used the QPSO-RF machine learning algorithm to study the extent of the cyanobacterial zone in Lake Taihu, revealing that the cyanobacterial bloom usually

begins to grow in the northwestern part of the lake, then spreads to the center of the lake, and dissipates earliest in the northwestern part. Literature [26] aimed to develop predictive models through evolutionary computation to provide early warnings of cyanobacterial outbreaks, showing that both spatially explicit and generalized models are suitable for most of the early warnings of cyanobacterial blooms, and developing a detailed understanding of the environmental conditions of cyanobacterial growth in Lake Taihu. Literature [27] embedded the relevant processing program into EarthEngine to develop an actionable workflow for monitoring cyanobacterial blooms, and utilized this process to measure the spatial and temporal patterns of cyanobacterial blooms in Lake Taihu, revealing that the pattern of cyanobacterial blooms in Lake Taihu is characterized by obvious spatial and temporal differentiation. Literature [28] collected long-term water quality and ecological indicators of Lake Taihu, examined the environmental evolution of the lake ecosystem, and emphasized that the evolution of the Lake Taihu basin is affected by the complex nonlinearity of the basin's biological, physical, chemical, and socioeconomic factors. Literature [29] proposed a CNN-LSTM integrated cyanobacterial bloom area prediction model and applied it to the prediction of cyanobacterial bloom area in Lake Taihu, indicating that the cyanobacterial bloom in Lake Taihu is correlated with the temperature, relative humidity, wind speed, and precipitation, revealing the effectiveness of the CNN-LSTM model. Literature [30] described the progress of remote sensing research on cyanobacterial blooms in inland waters, including the optical properties of cyanobacteria, chlorophyll, etc., and the application of satellite imaging, and concluded that the remote sensing algorithms for cyanobacterial pigmentation have made many significant advances, and that the application of satellite imagery has greatly improved the understanding of the mechanism of cyanobacterial bloom driving. The above study describes the serious impacts of cyanobacterial blooms on Lake Taihu and its surroundings, and proposes methods and models for predicting or detecting cyanobacterial blooms on Lake Taihu using satellite imaging, machine learning algorithms, and cloud computing platform images.

This paper firstly describes the basic situation of Taihu Lake region and clarifies the necessity of establishing a dynamic early warning model for cyanobacterial bloom in Taihu Lake. Secondly, MODIS satellite remote sensing and Landsat 8 satellite remote sensing monitoring results are used as the data basis for dynamic detection, and the normalized vegetation algorithm is selected and optimized, combined with water temperature remote sensing inversion as the identification and detection algorithm of cyanobacterial bloom. Subsequently, by extracting the main features of cyanobacterial blooms, analyzing the spatial and temporal changes of cyanobacterial blooms, and combining with the LightGBM algorithm, a set of dynamic early warning models for cyanobacterial bloom outbreaks in Lake Taihu is constructed. The model is used to develop a continuous all-weather temporal and spatial forecasting of the Lake Tai cyanobacterial bloom, and analyze the temporal and spatial characteristics of its intra-day change process.

2. Overview of Taihu Lake

Lake Taihu is the third largest freshwater lake in China and one of the five largest freshwater lakes in the middle and lower reaches of the Yangtze River, located in the Yangtze River Delta Plain. The geography of Lake Taihu is shown in Figure 1, with its latitude and longitude ranging from 30°55′ 40″ ~31°32′ 58″ N, 119°52′ 32″ ~120°36′ 10″ E, with an area of 2,427.8km², including 51 islands, with an average water depth of 1.9m, and the maximum water depth of nearly 3m, which is a typical inland large-scale shallow water lake. Centered on Taihu Lake, the entire Taihu Lake basin spans Zhejiang, Jiangsu and Shanghai provinces and cities, and is one of the most densely populated and economically developed areas in China. However, in recent years, along with the rapid economic development, the ecological environment of the basin continues to deteriorate, and the problem of eutrophication of Lake Taihu is becoming more and more serious.

As can be seen from Figure 1, Lake Tai can be divided into nine lake areas from west to east: the

western littoral zone, the southern littoral zone, the center of the lake, Zhushan Bay, Meiliang Bay, Gonghu Bay, the eastern littoral zone, and East Taihu Lake. According to the 2012 Annual Water Resources Bulletin of Taihu Lake Basin and Southeast Rivers, the water quality of East Taihu Lake, East Coastal Area and Wuli Lake is IV in the whole year, with a total of 446.2 square kilometers, accounting for 19.1% of the whole lake area, Gonghu Lake is V, with a total of 163.8 square kilometers, accounting for 7.0%, and the rest of the lake area is worse than V, with a total of 1,728.0 square kilometers, accounting for 73.9%. Lake Taihu is moderately eutrophic during the whole year, and the lakes are moderately eutrophic in Meiliang Lake, Zhushan Lake, the center of the lake, the western littoral zone and the southern littoral zone, accounting for 73.9% of the area of the lakes, and the other lakes are mildly eutrophic, accounting for 26.1%. It can be seen that the task of managing cyanobacterial bloom in Taihu Lake has been urgent, and it is necessary to establish a remote sensing monitoring system for cyanobacterial bloom outbreaks to lay a foundation for the realization of early warning and prediction of the bloom.

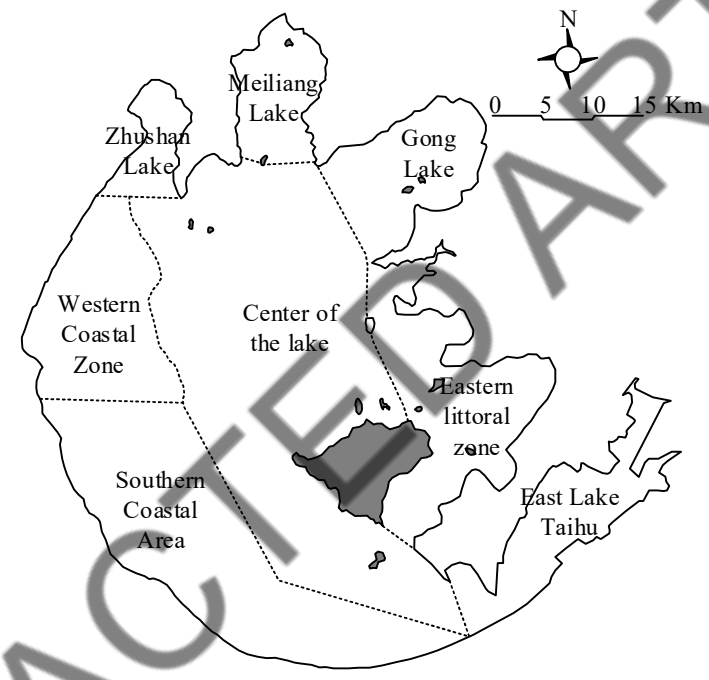

Fig. 1. Taihu lake subregion

3. Algorithms for dynamic detection of cyanobacterial blooms

This chapter describes the acquisition and pre-processing process of MODIS and Landsat 8 satellite remote sensing data, compares the two cyanobacterial bloom identification methods and selects the optimized NDVI threshold identification method, and realizes the remote sensing inversion of water temperature with the single-window and split-window algorithms, so as to launch the dynamic detection of cyanobacterial bloom in Taihu Lake region.

3.1. Optical Remote Sensing Image Data Acquisition and Preprocessing

As the main means of surface information acquisition, remote sensing satellite technology imaging is based on its mounted visible light camera, imaging spectrometer and other instruments, the satellite will be acquired by the surface information for preliminary processing, transmitted to the ground receiving station, the received image data for transformation, correction and other work, to generate image data for different purposes. This section describes the remote sensing data and pre-processing processes and methods of MODIS and Landsat 8 satellites respectively, which are derived as the

principles of remote sensing detection of cyanobacterial bloom in Taihu Lake.

3.1.1. MODIS satellite remote sensing data and pre-processing. EOS satellite is the abbreviation of a series of satellites planned to be launched by the U.S., and the MODIS data used in this paper are included in them.Terra/MODIS satellite has been launched successfully since 1999, and has been continuously used for surface observation, climate change analysis and other researches. This satellite passes through China at about 10:30 a.m., 705 km from the ground, and the Aqua/MODIS satellite was launched in 2002 and passes through China at about 13:30 a.m. Therefore, the two satellites can realize daily observations of the earth's surface and climate change. Therefore, the two satellites can realize two observations of the ground per day.The maximum spatial resolution of MODIS data is 250m, and the number of bands is 36, covering the range from visible light to thermal infrared. Among all the free satellite data, MODIS has a long history of use and rich experience in remote sensing of water bloom monitoring because of its easier access and larger data volume (two days return).

MODIS data preprocessing mainly includes geometry correction, area cropping, reflectance conversion, Rayleigh scattering correction, and cloud mask, as shown below:

1) Geometry Correction. The positional offset and image deformation of MODIS data are very large, and the first step of geometric correction is very necessary. In this paper, we utilize the MCTK plug-in in ENVI software to directly complete the geometric correction of MODIS data.

2) Area Cropping. In order to reduce the impact of redundant image data on the processing and improve the efficiency of data processing, this paper crops the geometrically corrected image data and only retains the image data of the Taihu Lake waters, and the subsequent image processing is based on the cropped image data.

3) Reflectance conversion. After the MCTK geometric correction, when the MODIS data are opened by ENVI software, the original DN values of all bands in the image are converted into two datasets in the form of radiance values and reflectance. In order to get the atmospheric apparent reflectance (ρ_{TOA}) needed for the subsequent extraction of cyanobacterial blooms, it is necessary at this time to first carry out the reflectance conversion work to convert all the pixels in the image to atmospheric apparent reflectance, which is converted as in Equation (1):

$$\rho_{roA} = \mathrm{Re}\ flec\ \tan ce / \cos\theta_0 \tag{1}$$

where θ_0 is the solar zenith angle.

4) Rayleigh scattering correction. In this paper, when using MODIS data for cyanobacterial bloom extraction, the bands used are red and near-infrared bands, and the NDVI algorithm belongs to the band ratio algorithm, which is able to reduce the error brought by atmospheric radiation to a certain extent, while MODIS data want to eliminate atmospheric errors and carry out accurate atmospheric correction work is more difficult, therefore, the preprocessing of MODIS is not carried out in this section for the atmospheric correction, only the Rayleigh scattering correction is applied to the data. The correction is shown in equation (2):

$$\rho_{TOA\text{-}Raylecigh} = TOA\_\ \mathrm{Re}\ flec\ \tan ce * T_g^{H_2O} / T_g - \rho_s \tag{2}$$

where T_g is the absorbing gas transmittance, $T_g^{H_2O}$ is the water vapor absorption transmittance, and ρ_t is the Rayleigh scattering reflectance obtained using the 6S radiative transfer model.

5) Cloud mask. Since the optical image data are susceptible to the influence of clouds and fog, the presence of clouds will cover the complete water surface of Lake Taihu thus affecting the extraction accuracy of the water bloom, so it is necessary to remove the thin clouds first when carrying out cyanobacterial water bloom extraction. In this paper, according to the existing research, a single-band thresholding algorithm is utilized to remove the thin clouds over the lake surface, and the area with Rrc(1640)>0.03 is identified as a cloud and eliminated.

3.1.2. Landsat 8 satellite remote sensing data and pre-processing. Launched successfully in 2013, Landsat 8 is the eighth satellite of the United States Landsat program and is equipped with the Land Imager (OLI) and the Thermal Infrared Sensor (TIRS). The satellite has 11 bands, of which bands 1-7 and 9-11 have a spatial resolution of 30m, while band 8 is a panchromatic band with a spatial resolution of 15m, and Landsat 8 has a revisit period of 16 days. Since its successful launch, this satellite has been widely used in the fields of resource investigation, environmental protection, disaster monitoring, etc. The preprocessing of Landsat 8 data mainly includes regional cropping, radiometric calibration and atmospheric correction, as shown below:

1) Regional cropping. In order to reduce the impact of redundant image data on the processing and improve the rate of data processing, this paper will crop the image data after geometric correction, and only retain the image data of the Taihu Lake waters, and the subsequent image processing is based on the cropped image data.

2) Radiometric Calibration. Since the ENVI software has built-in correlation coefficients for radiometric calibration of Landsat satellites, the radiometric calibration function of the software can be used to perform automatic radiometric calibration of Landsat 8 data.

3) Atmospheric Correction. In this section, the atmospheric correction module of ENVI software Flaash is used to correct the images. Flaash uses the MODRTAN radiative transfer model as the kernel to calculate the atmospheric parameters of the reflectance inversion model, and estimates the atmospheric attributes through the spectral features of the image pixels to realize the image pixel-level correction.

3.2. Introduction to common vegetation indices

The spectral characteristics of vegetation are obvious and unique: due to the role of chlorophyll, there is a reflection peak in the green band of visible light, while the absorption valley is formed in the blue and red light, affected by the structure of leaf cells, in the near-infrared wavelengths to form a vegetation-specific “land-slope effect”, the reflectance is greatly increased, and therefore the use of the near-infrared and visible wavelengths for linear or non-linear combination of operations to form a vegetation index that can reflect the distribution and growth of green vegetation on the surface of the earth. Therefore, the linear or non-linear combination of near-infrared and visible light bands is used to form a vegetation index that reflects the distribution and growth of green vegetation on the surface. Since the reflectance spectral characteristics of cyanobacterial blooms are similar to those of green vegetation, it is possible to distinguish between cyanobacteria and other features by calculating the vegetation index, and then extract information about cyanobacteria by setting a threshold value.

In the following, two common vegetation indices are introduced, and their effects on the identification and extraction of cyanobacterial bloom information are analyzed to select the optimal algorithm.

3.2.1. Ratio Vegetation Index (RVI). Due to the large difference in reflectance of green vegetation in the near-infrared and red light bands, the Ratio Vegetation Index (RVI) is defined as in equation (3):

$$RVI = \rho_{nit} / \rho_{red} \tag{3}$$

Eqs. ρ_{nit} and ρ_{red} represent the reflectance in the near-infrared and red light bands, respectively. Specific vegetation index (SVI) is closely related to vegetation LAI, leaf dry biomass and chlorophyll content, and is widely used to detect and calculate vegetation biomass. Areas covered with healthy green vegetation have Specific Vegetation Index (SVI) values much greater than 1 due to the strong absorption in the high infrared and red light bands, whereas clean water, buildings, bare soil, or vegetation with severe pests and diseases usually have SVI values less than 1. On lakes with dense cyanobacterial cover, the SVI is generally greater than 2, and if the cyanobacteria are particularly sparse, the SVI is generally near 1. The sensitivity of the RVI is dependent on the state of the vegetation cover and is very sensitive when the cover is high, while the sensitivity decreases significantly when the surface vegetation cover is less than 50%. Specific vegetation indices are susceptible to atmospheric conditions, so in general the images should be atmospherically corrected to obtain the true reflectance of the surface for calculation.

3.2.2. Normalized Vegetation Index (NVI) and Enhanced Vegetation Index (EVI). Considering the problem of the infinite increase of the ratio vegetation index due to the fact that the near-infrared reflectance of the particularly lush vegetation is much higher than the reflectance of the red light band, the normalized vegetation index (NDVI) with a value field of $(-1 \sim 1)$ is used as in Eq. (4):

$$NDVI = (\rho_{nir} - \rho_{red}) / (\rho_{nir} + \rho_{red}) \tag{4}$$

where ρ_{nir} and ρ_{nir} represent the reflectance in the near-infrared and red light bands, respectively. The normalized vegetation index (NVI) obtained by normalization of the ratio vegetation index can, to a certain extent, eliminate the effects caused by changes in the sensor observation angle, solar altitude angle, topography, and atmosphere-related radiant illumination, and is more sensitive to the response of the vegetation.

Normalized vegetation index is widely used in the fields of surface vegetation cover and crop growth detection. When the ground surface is covered by green vegetation, the NDVI is generally positive, and the value increases with increasing coverage. For surfaces covered by clouds, water, snow, etc., which have a large visible light reflectivity, the NDVI is generally negative. The normalized vegetation index reflects the difference between the near-infrared and red light bands in a nonlinear way, and this nonlinear stretching results in increased sensitivity to low-covered areas and decreased sensitivity to high-vegetation areas, and with the increase in the density of vegetation on the surface, the normalized vegetation index is easy to saturate, and synchronous growth can not be achieved. It has been proved that the advantage of using NDVI will be more obvious in the mid-growth of crops or in the case of medium vegetation cover.

In order to solve the deficiencies of Normalized Vegetation Index (NVI), Enhanced Vegetation Index (EVI) using MODIS sensor is shown in equation (5):

$$EVI = 2.5 \times \frac{\rho_{nir} - \rho_{red}}{\rho_{nir} + C_1 \rho_{red} + L - C_2 \rho_{blue}} \tag{5}$$

where ρ_{nir}, ρ_{red} and ρ_{blue} are the reflectance of near-infrared, red and blue light bands, respectively, C_1 and C_2 are the atmospheric correction parameters for red and blue light, with values of 6 and 7.5, respectively, and L is the soil conditioning parameter 1. The enhanced vegetation index, with the introduction of the atmospheric correction parameter and the soil conditioning parameter, can effectively make up for the shortcomings of the normalized vegetation index, increase the sensitivity to the high-vegetation-covered areas, and reduce the influence of the atmosphere to a greater extent to improve the monitoring of vegetation by weakening the background signal of the vegetation canopy and soil changes. It can also improve the monitoring of vegetation by weakening the background signal of vegetation canopy and soil variations by

minimizing the influence of the atmosphere.

3.3. Remote sensing inversion of water temperature

The data sources used for remote sensing inversion of water temperature in this section include MODIS thermal infrared and the RS sensor carried by HJ-1B star. Among them, MODIS image recognizes water temperature by applying split-window algorithm, and HJ-1B thermal infrared image recognizes water temperature by applying single-window algorithm.

3.3.1. Single Window Algorithm. The equation for the transmission of surface thermal radiation through the atmosphere systematizes the sources of the total amount of radiation received by the IRS, covering the thermal radiation from surface objects, the upward radiation from the atmosphere and the downward portion of the radiation. Thermal radiation is also subject to the physical process of attenuation due to its absorption by the atmosphere as it passes through it. Therefore, the attenuation of surface radiation and atmospheric radiation is an important factor in the transmission of thermal radiation, and the surface temperature is calculated by physical modeling of the radiation transmission process.

For the relationship between radiation intensity, temperature and wavelength, the Planck radiation function is shown in Eq. (6) through the abstract concept of the blackbody as a benchmark:

$$B_\lambda(T) = \frac{c_1}{\lambda^5\left(e^{c2/\lambda T}-1\right)} \tag{6}$$

where $B_\lambda(T)$ is the abstract concept its own actual radiation intensity, expressed in units of $W\cdot m^{-2}\cdot sr^{-1}\cdot \mu_m{}^{-1}$. λ is the wavelength. C1 and C2 are the radiation constants, $C1 = 1.19104356*10^{-6} W\cdot m^{-2}$ and $C2 = 1.4387685*10^{4}\mu_m\cdot K$. T is the temperature (K).

By analyzing the process of radiation transmission in the atmosphere affecting the action of the radiation intensity received by the satellite sensor as in equation (7):

$$B_i\left(T_i\right) = \tau_i(\theta)\left[\varepsilon_i B_i\left(T_s\right) + \left(1-\varepsilon_i\right) I_i\downarrow\right] + I_i\uparrow \tag{7}$$

where T_s is the surface temperature. T_i is the brightness temperature on the star. $\tau_i(\theta)$ refers to the atmospheric transmittance at the sensor observation angle of θ in the shooting attitude of the satellite, and ε_i is the specific emissivity of the target water body. $B_i\left(T_i\right)$ is the intensity of thermal infrared radiation measured by the sensor in band i, and $I_i\uparrow$ and $I_i\downarrow$ are the upward and downward thermal radiation of the ground target, respectively.

Parameters $I_i\uparrow$, $I_i\downarrow$ and $\tau_i(\theta)$ required for the inversion of the IRS data of HJ-1B in this paper are available on the NASA website, and the corresponding parameter values can be calculated from the sensor's shooting time, latitude, longitude, and atmospheric type of the target area, and the sensor's response curve on the corresponding NASA website.

3.3.2. Split Window Algorithm. There are a total of eight bands in the thermal infrared spectral interval of the MODIS sensor, and the thermal infrared bands mainly used in the water body temperature inversion are band31 and band32.The core expression of the split-window remote sensing temperature inversion model for the two thermal infrared bands is shown in Equation (8):

$$T_s = A_0 + A_1 T_{31} - A_2 T_{32} \tag{8}$$

where T_s denotes the actual temperature of the ground object (K), T_{31} and T_{32} denote the brightness temperature values of band31 and band32 in the remote sensing image data, which are calculated by substituting the values after radiative calibration of band31 and band32 in the

compilation process of the program. A_0, A_1 and A_2 are the parameters of the split window algorithm, defined as Eqs. (9)-(11):

$$A_0 = \left[\frac{D_{32}\left(1-C_{31}-D_{31}\right)}{D_{32}C_{31}-D_{31}C_{32}}\right]a_{31} - \left[\frac{D_{31}\left(1-C_{32}-D_{32}\right)}{D_{32}C_{31}-D_{31}C_{32}}\right]a_{32} \tag{9}$$

$$A_1 = 1+\frac{D_{31}}{D_{32}C_{31}-D_{31}C_{32}} + \left[D_{32}\left(1-C_{31}-D_{31}\right)/\left(D_{32}C_{31}-D_{31}C_{32}\right)\right]b_{31} \tag{10}$$

$$A_2 = \frac{D_{31}}{D_{32}C_{31}-D_{31}C_{32}} + \left[D_{31}\left(1-C_{32}-D_{32}\right)/\left(D_{32}C_{31}-D_{31}C_{32}\right)\right]b_{32} \tag{11}$$

where a_{31}, b_{31}, a_{32} and b_{32} are constants and can be taken as $a_{31}=-64.60363$, $b_{31}=0.440817$, $a_{32}=0-68.72575$, $b_{32}=0.473453$. Other intermediate parameters are calculated as in Eqs. (12)-(13):

$$C_i = \varepsilon_i \tau_i(\theta) \tag{12}$$

$$D_i = \left[1-\tau_i(\theta)\right]\left[1+\left(1-\varepsilon_i\right)\tau_i(\theta)\right] \tag{13}$$

where i refers to bands 31 and 32 of MODIS. $\tau_i(\theta)$ is the atmospheric transmittance for viewpoint θ. ε_i is the surface specific emissivity for band i.

The atmospheric transmittance $\tau_i(\theta)$ is a key influence factor in the inversion process of target feature temperature, which is generally converted by atmospheric water vapor content. In this paper, band2 and band19 of remote sensing image data are used to calculate the atmospheric water content over the target area, based on which its correlation coefficient with the atmospheric transmittance is used to estimate $\tau_i(\theta)$ with equation (14):

$$\omega = \left[\frac{\alpha - \ln\frac{\rho_{19}}{\rho_2}}{\beta}\right]^2 \tag{14}$$

where ω is the atmospheric moisture content $\left(g\cdot cm^{-2}\right)$, α and β are constants taken as $\alpha=0.02$ and $\beta=0.6321$, respectively. ρ_{19} and ρ_2 are the surface reflectance of band19 and band2 in MODIS, respectively.

There is a significant linear correlation between the atmospheric moisture content and $\tau_i(\theta)$, which can be converted by the corresponding simulation equations. The atmospheric transmittance is estimated by the segmented regression equation in the IDL temperature inversion program to facilitate the calculation.

The atmospheric transmittance is not only determined by the atmospheric moisture content, but also influenced by several factors, including the sensor viewing angle and the atmospheric profile temperature. Therefore, it is necessary to correct for the viewpoint of the sensor flight attitude and the temperature using different temperature intervals by applying the kernel correction to $\tau_i(\theta)$. The core correction is shown in Eq. (15):

$$\tau_i'(\theta) = \tau_i(\theta) + \delta\tau_i(T) - \delta\tau_i(\theta) \tag{15}$$

where $\tau_i'(\theta)$ is the atmospheric transmittance of the $i(i=31,32)$ nd band after perspective correction. $\tau_i(\theta)$ is the atmospheric transmittance of the satellite at the moment of shooting in the under-star position. $\delta\tau_i(T)$ is the temperature correction function for the two bands of the sensor. $\delta\tau_i(\theta)$ is the viewing angle correction function of band31 and band32 in MODIS image, and its function is expressed as equation (16):

$$\delta\tau_i(\theta) = -0.00322 + \left(3.0967\times10^{-5}\right)\theta^2 \tag{16}$$

4. Construction of an early warning model for cyanobacterial bloom dynamics

4.1. Characterization of cyanobacterial blooms

For cyanobacterial blooms, the real-time dynamic changes are large, and it is easy to change its spatial location and distribution by wave movement and wind force. Therefore, it can be started from spectral characteristics, environmental indicators, etc. This paper synthesizes the spectral performance of each wave band and the influence on its growth environment to mine the characteristic information of cyanobacterial blooms, with a view to distinguishing cyanobacterial blooms. The coupled image of HJ-1-CCD band of Taihu Lake wave on December 14, 2013 is used in this section.

4.1.1. Image Characterization of Cyanobacterial Blooms. Cyanobacterial blooms significantly increase the chlorophyll content in the water body, leading to changes in the spectral characteristics of the water body. Figure 2 shows the measured reflectance data of five sample points in Taihu Lake, Wuxi City, on December 14, 2013, which were collected in the field outside the drinking water source in Wuxi City. The figure shows that at wavelengths between 350nm and 500nm, the strong absorption of algae and soluble organic matter (CDOM) in the water body causes relatively low remote sensing reflectance values. Starting from 350nm, the remote sensing reflectance increases with increasing wavelength. There is a reflectance peak near 550 nm, which is formed due to the weak absorption of algal chlorophylls and carotenoids as well as scattering by the cells. A trough in reflectance occurs near 660 nm, caused by the absorption of chlorophyll. There is an obvious reflectance peak at 700nm, which is the most significant spectral feature of algal-containing water bodies, and its presence or absence is usually the basis for determining whether the water body contains algal chlorophyll.

The spectral patterns of different states of algal bloom are consistent, with different reflectance sizes. The reflectance of the bloom covering the surface of the water body in the form of lacquer is high, such as the bloom 1 in the figure, and the reflectance of the bloom with low algal concentration and suspended on the water surface is low, such as the bloom 2 in the figure, and the water body has the lowest reflectance over the whole spectral interval and the spectral pattern is flat. The spectral curve morphology of aquatic plants is similar to that of the water bloom, with the difference being in the magnitude of the reflectance values. There are differences in the reflectance values of different types of aquatic plants. Aquatic plant 1 is a floating leaf plant with higher reflectance, and aquatic plant 2 is a submerged plant, which is more affected by the water body and has lower reflectance. The spectral patterns of blooms and aquatic plant 1 are similar, and blooms that are very thickly attached to the water surface, such as bloom 1, have a higher reflectance than aquatic plants, but blooms with lower algal concentrations have a lower reflectance than floating-leaf plants.

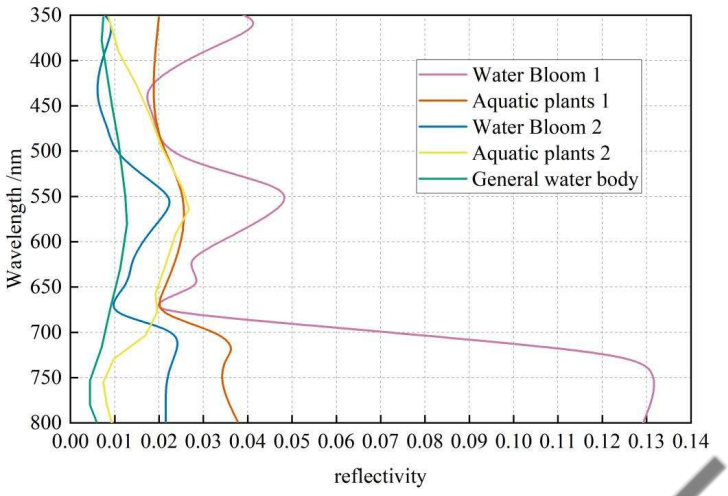

Fig. 2. Measured reflectance curve of Taihu Lake on December 14, 2013

4.1.2. Distinguishing cyanobacterial blooms from terrestrial information. The relative reflectance values of each type of feature in each band were counted, and the average value was used to represent the relative reflectance value of the feature in each band, and the spectral curves of the features were plotted in Fig. 3. The characteristics of the three curves of cyanobacterial blooms, aquatic plants and terrestrial vegetation were consistent, and the cyanobacterial blooms showed a decrease in the reflectance in the blue and red light, and a high reflectance in the green light with a small reflectance peak of 0.8, which is in agreement with the spectral characteristics of the actual measurement above. The near-infrared band has obvious vegetation characteristics "steep slope effect", reflectivity increased. For water bodies without algae, the relative reflectance values decrease from B1 to B5. In general, the difference in spectral characteristics between cyanobacteria-covered water bodies and algae-free water bodies is more obvious. The spectral curves of the construction site showed an increasing trend from B3 to B5, contrary to the other features.

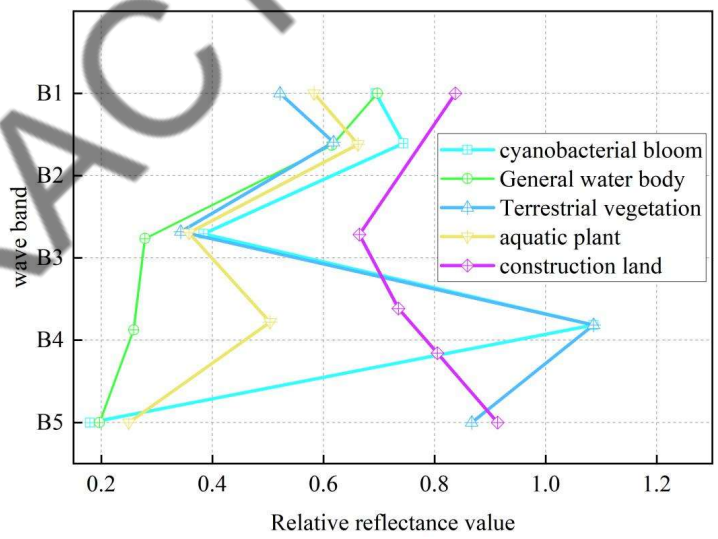

Fig. 3. Spectral characteristics of typical features

4.2. Spatial and temporal variability of cyanobacterial blooms

The algorithm proposed in Chapter 3 of this paper was used to batch process all environmental satellite images to obtain the total area and distribution of cyanobacterial blooms extracted from each image, in order to carry out the research on the spatial and temporal characteristics of

cyanobacterial blooms in Lake Taihu.

Taking the maximum area of cyanobacterial bloom per month as the area of cyanobacterial bloom in that month, the statistics of all the selected images for the area of cyanobacterial bloom during the second half of 2010-2015 are shown in Fig. 4, which shows that there are few images that meet the requirements in summer, especially in July, mainly because of cloudy and rainy weather in summer, but from the only images, it can be seen that in 2014 and 2015, the July Lake Taihu cyanobacterial bloom outbreaks were smaller in area and the water body was in better condition. Autumn is the most serious season for cyanobacterial bloom in Lake Taihu, the area of cyanobacterial bloom in autumn is the largest, in which the most serious bloom is in August and September, this is because under the condition of sufficient nutrient salts, the temperature and light are the main factors affecting the cyanobacterial bloom. In summer, after the temperature exceeds 35 degrees, the cyanobacteria will be more inclined to be under the surface of the water because they are afraid of heat. In the fall, due to the suitable temperature, the cyanobacteria particles float on the surface of the water, and the bloom is in large scale. In winter, the area of cyanobacterial bloom decreased slightly compared with that of fall but still existed because the deterioration of the water environment of the lake in recent years led to the growth of the duration of cyanobacterial bloom.

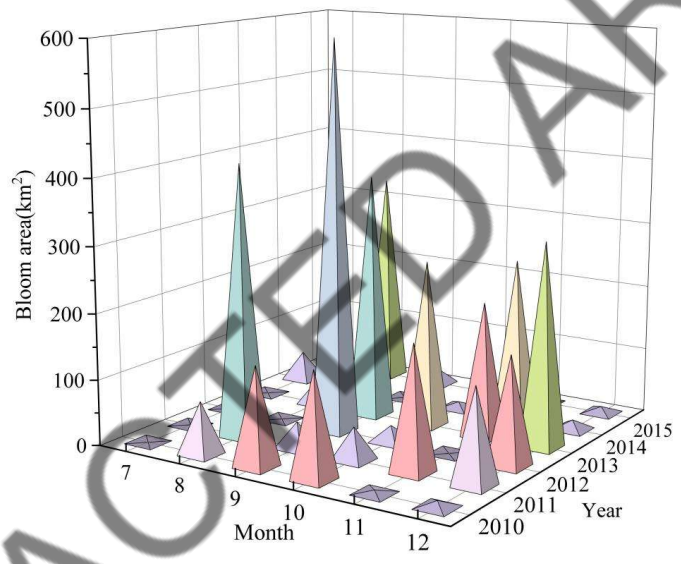

Fig. 4. Comparison of cyanobacteria bloom area between moons

Figure 5 shows the trend of the cyanobacterial bloom area in Lake Taihu between 2010 and 2015 with the available data. It can be seen that the water quality of Lake Taihu showed a downward trend from 2010, the cyanobacterial bloom outbreaks intensified and the area increased, reaching a maximum value of 586km^2 in 2012. However, the water quality has improved since 2014, and the area of cyanobacterial bloom in Lake Taihu was small and the water body was in good condition in 2014 and 2015, which has a significant relationship with the high attention paid by the government as well as the environmental management measures taken, which has invested a lot of manpower and financial resources to manage the water quality and improve the water environment, and the research work of scholars has also provided the government with the support of the decision-making. A great deal of publicity and news reports have also made people realize the consequences of environmental degradation, and the concept of protecting the water environment has been deeply rooted in people's hearts.

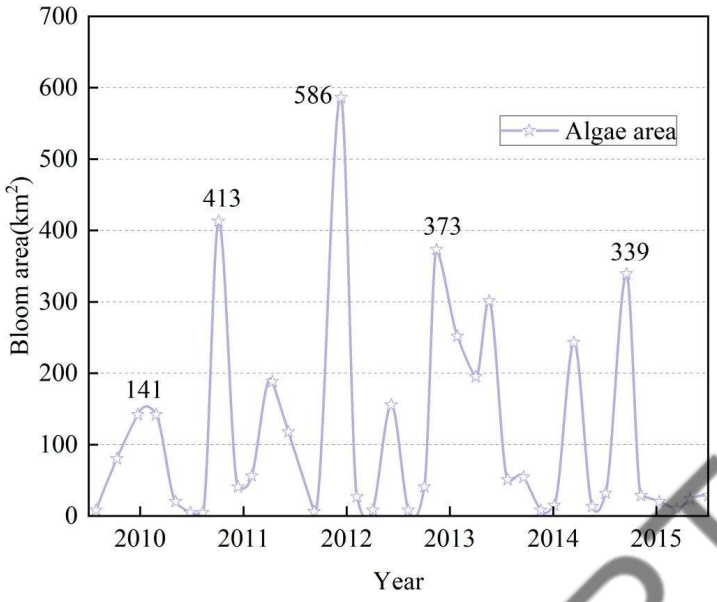

Fig. 5. Comparison of cyanobacteria bloom area between years

4.3. Accuracy Assessment and Selection of Cyanobacterial Bloom Prediction Models

Continuous all-weather monitoring of the intra-day change process of cyanobacterial blooms is an important basis for realizing regional early warning of the dynamics of cyanobacterial blooms. However, due to the influence of observation conditions and time resolution of the data, it is still impossible to realize the all-weather continuous monitoring of intra-day changes of cyanobacterial blooms in lakes only by relying on the effective observation data from long time series satellites. In this paper, a machine learning method is introduced to break through the limitations of remote sensing technology in all-weather continuous monitoring.

4.3.1. LightGBM-based cyanobacterial bloom prediction models. It can be seen from the above study that the MODIS satellite observation with a 2-day return provides a possibility for monitoring the intraday dynamics of cyanobacterial blooms in lakes. However, the effective observation data from satellites are usually time-discontinuous due to the influence of observation conditions such as cloudy and rainy weather and nighttime. In addition, how to obtain the intraday dynamics of cyanobacterial blooms outside the observation moment of MODIS satellites is still a difficult problem. Therefore, how to realize all-weather continuous monitoring of cyanobacterial bloom outbreaks in lakes under the premise of retaining the advantages of satellite remote sensing data in spatial resolution as much as possible is the key to realizing the prevention and control of regional cyanobacterial bloom disaster dynamics. To this end, some scholars have constructed prediction models based on the linear or nonlinear relationships between different meteorological variables and cyanobacterial blooms, using data-driven methods such as deep learning and machine learning to fill in the data of cyanobacterial blooms, which provides a new way of thinking for the spatial and temporal continuous monitoring of the intra-day changes of cyanobacterial blooms in lakes. However, most of these prediction models rely on actual station data, and it is difficult to retain the temporal and spatial advantages of the generated cyanobacterial bloom data at the same time. The Landsat 8 satellite reanalysis meteorological dataset provides information on the changes of multiple meteorological variables (e.g., precipitation, wind speed, and temperature) at 24 moments throughout the day at a global scale with a spatial resolution of 9 km, which enables all-weather monitoring of the changes of meteorological conditions in the region. Therefore, this paper will combine the advantages of MODIS satellite data and Landsat 8 satellite data in terms of spatial and temporal resolution, and utilize the machine learning (LightGBM) method to realize the all-weather

spatial and temporal continuous monitoring (forecasting) of cyanobacterial blooms in lakes by constructing meteorological data-driven cyanobacterial bloom prediction models.

After the model variables and model structure are determined, all input data are divided into training set (70%), validation set (10%) and test set (20%). In this case, to ensure that both morning and afternoon test results are available, one morning moment (09:00) and one afternoon moment (14:00) data fixation are fixedly selected as the test set. Combining the cyanobacterial bloom area data and meteorological data at eight moments per day (08:00 to 15:00 local time, UTC+8), the relationship between model variables was simulated and mined using the LightGBM method. And after the model training was completed, the Pearson correlation coefficient (R) and root mean square error (RMSE) of each image element were calculated using the corresponding validation set or test set data. Based on the comparison of the model test results, the model with the best prediction performance is selected and inputted into the all-weather gridded meteorological data to make all-weather spatial and temporal continuous prediction of the cyanobacterial bloom area in Lake Taihu. At this point, the construction and selection of the time-dependent prediction model for the cyanobacterial bloom area is completed.

4.3.2. Spatial and temporal characteristics of intraday cyanobacterial bloom processes. In order to analyze the spatial and temporal characteristics of the intraday change process of cyanobacterial bloom in Lake Taihu, this paper obtains the data covering the whole Lake Taihu and under the date of "at least one available MODIS image". Based on the comparative analysis of the model test results, the all-weather gridded meteorological data provided by ERA-5 Land are input into the model to realize the all-weather continuous forecast of the cyanobacterial bloom area in Lake Taihu from 2010 to 2015. To facilitate the understanding of the model's forecast results, Figure 6 provides the forecast results at five moments (local time, UTC+8) outside the MODIS observation period, which are distributed in different types of time periods such as morning, afternoon or night.

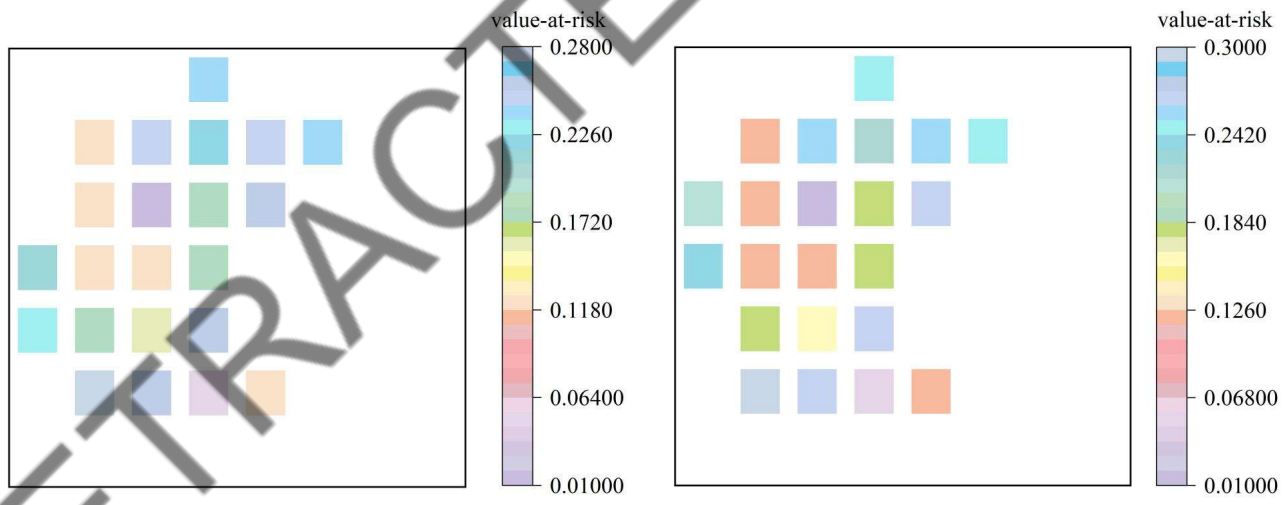

(a) 6:00 hours (b) 7:00 hours

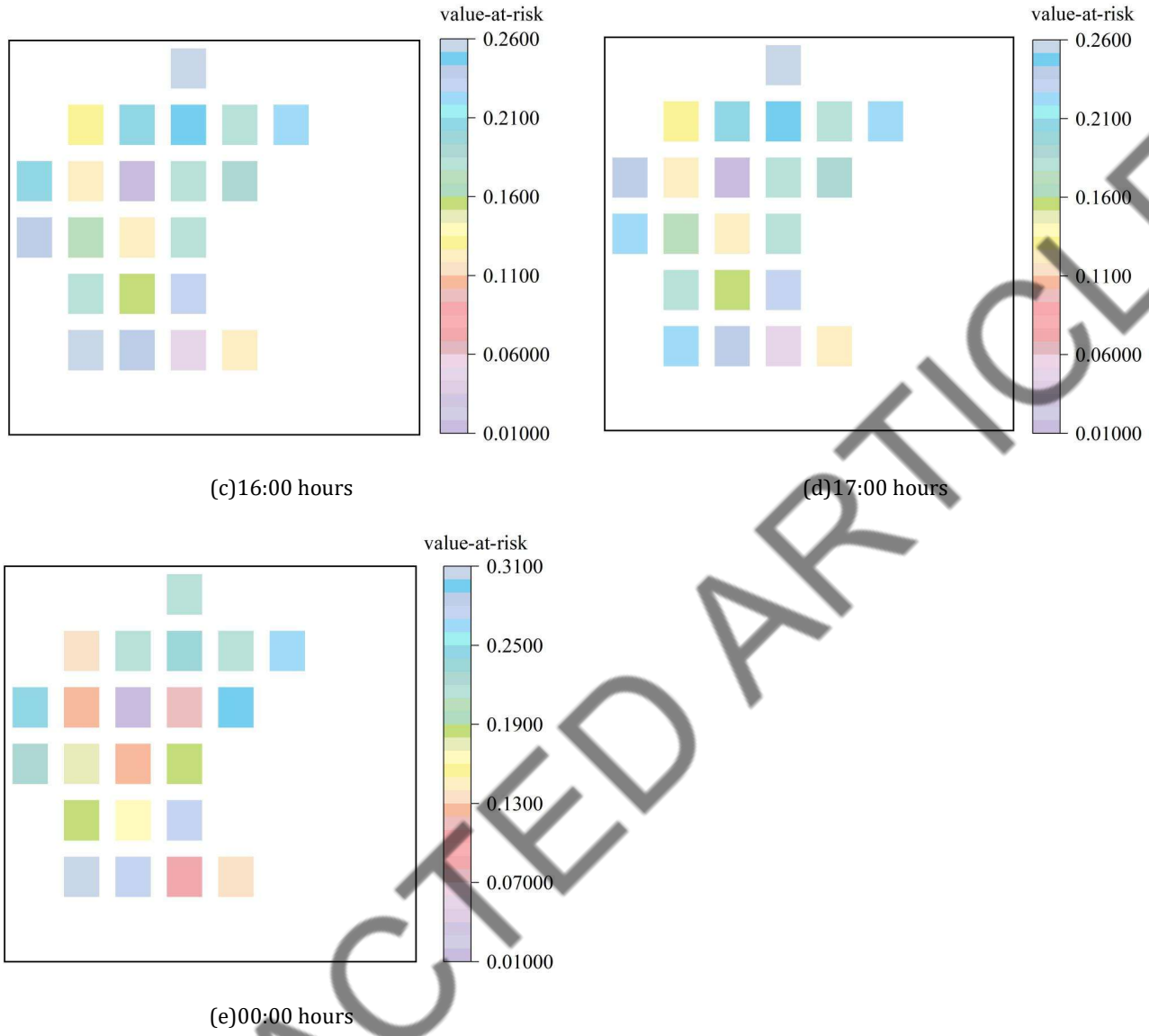

Fig. 6. Prediction results of cyanobacteria bloom outbreak area at five times

Combined with the all-weather forecasting results of the model, the long-term mean values of the cyanobacterial bloom area at 24 moments of the whole day were calculated, based on which its regional (the whole lake of Taihu and its six subregions) and seasonal (spring, summer, autumn, winter, 2011-2020) characteristics were statistically analyzed, and the results are shown in Figs. 7 and 8.The intraday change curves of the area of the cyanobacterial bloom are presented in Figs. 7 and 8. The six lake zones were Meilang Bay, Zhushan Bay, Gonghu Bay, the west and south shores of the lake, and the center of the lake.

The hourly monitoring results showed that the intraday variation curves of cyanobacterial bloom (bloom area) in Lake Taihu in different seasons had similar shapes, but there were differences in the range of intraday variations, which were characterized by the small peak of the bloom area in the morning (08:00-12:00), and the lower bloom area in winter than that in the rest of the three seasons. The results of the intra-day changes of cyanobacterial blooms (bloom area) in different seasons in Lake Taihu are shown in Figure 7.

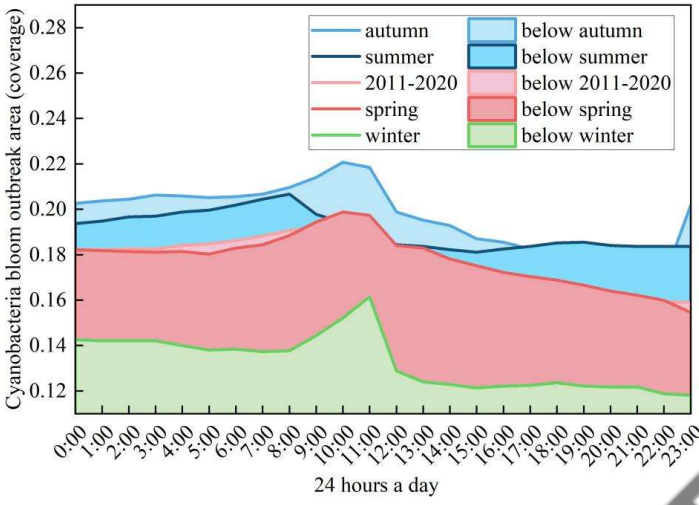

Fig. 7. Diurnal variation of cyanobacteria bloom outbreak area in Taihu Lake

The statistical results of the intra-day change curves of cyanobacterial blooms (bloom area) in six sub-areas of Lake Tai show that the overall seasonal difference is lower in winter than in the rest of the three seasons, and it is also observed that the bloom area in Meiliang Bay is higher than in the rest of the five sub-areas, and the results of the intra-day change of cyanobacterial blooms (bloom area) in different sub-areas of Lake Tai are shown in Fig. 8. In conclusion, the bloom area of Meiliang Bay is higher than that of the rest of the lake and lower than that of the rest of the season in winter. In conclusion, the overall area of cyanobacterial bloom in Meiliang Bay was higher than that in the rest of the lake, and the overall area in winter was lower than that in the rest of the season, and the changes of cyanobacterial bloom on longer time scales, such as daily/monthly, were more similar to the characteristics of these areas and seasons observed on hourly scales, which might be the cumulative result of the intra-day dynamics of cyanobacterial bloom. Therefore, continuous monitoring and regular analysis of the intra-day dynamics of cyanobacterial blooms and their risks are necessary to prevent the deterioration and accumulation of cyanobacterial blooms.

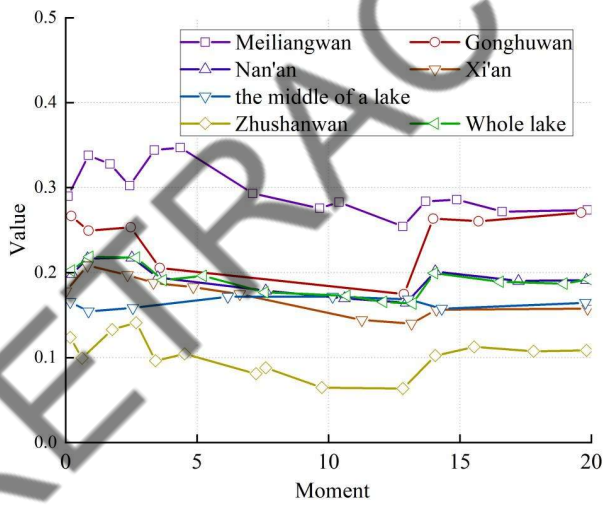

(a) Spring

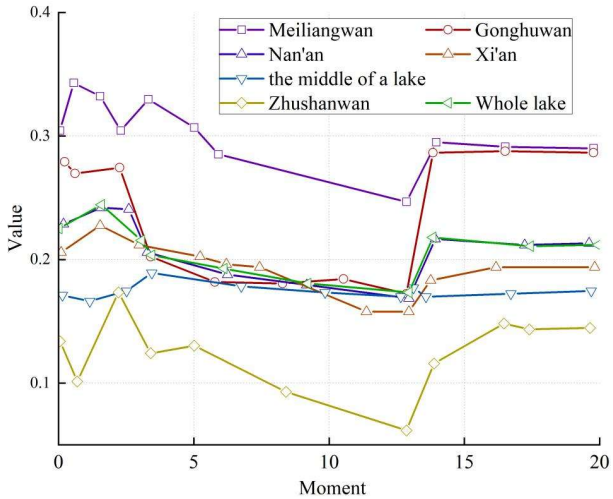

(b) Summer

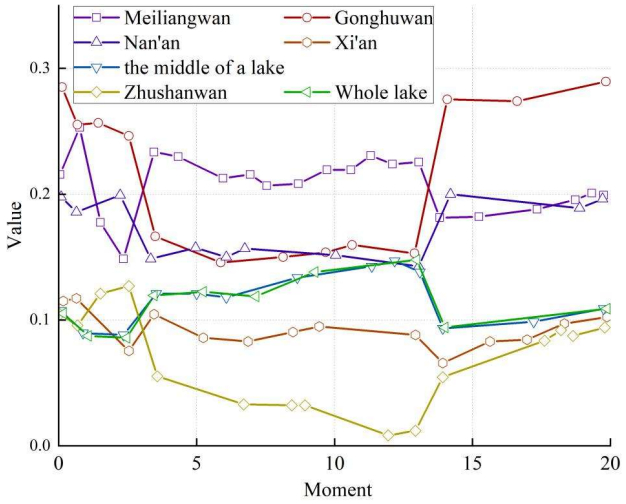

(c) Autumn

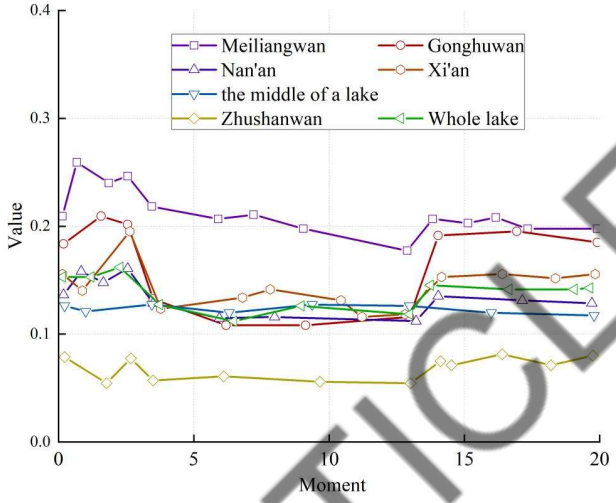

(d) Winter

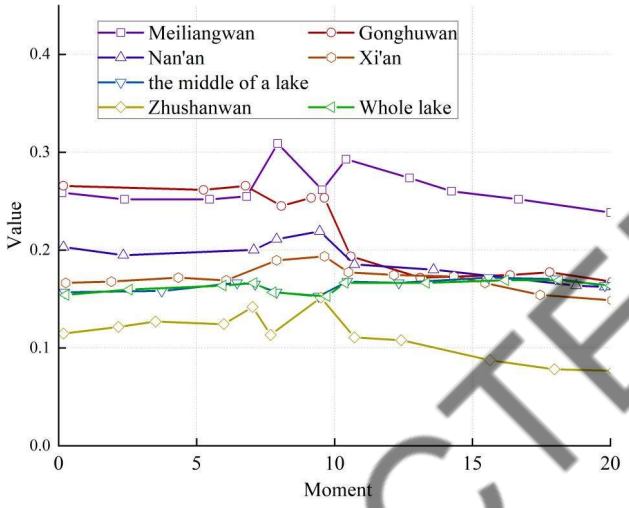

(e) 2011-2010

Fig. 8. Regional and seasonal characteristics of the outbreak area change curve

5. Conclusion

In order to meet the application requirements of dynamic monitoring of cyanobacterial bloom in Lake Taihu, this paper combines the long time series remote sensing satellite MODIS, Landsat 8 data and normalized vegetation index to extract the image and spatial and temporal features of cyanobacterial bloom, and realizes the construction of dynamic early warning model of cyanobacterial bloom in Lake Taihu based on the LightGBM method.

Comparison and summarization of the spatial and temporal differences of intraday changes of cyanobacterial bloom in Lake Taihu under different regions and seasons using the model in this paper revealed that the time period of intraday bloom was concentrated in 8:00 a.m. to 12:00 p.m., and the area of cyanobacterial bloom under the same partition and season had a similar pattern of time-to-time changes. Seasonally, the overall area of cyanobacterial bloom in winter was lower than that in the rest of the seasons, and the area of cyanobacterial bloom in fall was the highest. Regionally, the area of cyanobacterial bloom in Meilang Bay was lower than that in the rest of the subregion.

Based on the long time series remote sensing data, this paper explores the establishment of the use of technology for the identification, extraction and early warning of cyanobacterial blooms, and

innovates the monitoring, prevention and control technology of cyanobacterial blooms in the Taihu Lake region.

References

[1] Zhao, Q., & Wang, Q. (2021). Water ecosystem service quality evaluation and value assessment of Taihu Lake in China. Water, 13(5), 618.

[2] Li, L., Zhao, X., Liu, D., Song, K., Liu, Q., & He, Y. (2021). Occurrence and ecological risk assessment of PPCPs in typical inflow rivers of Taihu lake, China. Journal of Environmental Management, 285, 112176.

[3] Qin, B., Paerl, H. W., Brookes, J. D., Liu, J., Jeppesen, E., Zhu, G., ... & Deng, J. (2019). Why Lake Taihu continues to be plagued with cyanobacterial blooms through 10 years (2007–2017) efforts. Science Bulletin, 64(6).

[4] Shi, K., Zhang, Y., Xu, H., Zhu, G., Qin, B., Huang, C., ... & Lv, H. (2015). Long-term satellite observations of microcystin concentrations in Lake Taihu during cyanobacterial bloom periods. Environmental Science & Technology, 49(11), 6448-6456.

[5] Luo, Y., Yang, K., Yu, Z., Chen, J., Xu, Y., Zhou, X., & Yang, Y. (2017). Dynamic monitoring and prediction of Dianchi Lake cyanobacteria outbreaks in the context of rapid urbanization. Environmental Science and Pollution Research, 24, 5335-5348.

[6] Qin, X., Xia, W., Hu, X., & Shao, Z. (2022). Dynamic variations of cyanobacterial blooms and their response to urban development and climate change in Lake Chaohu based on Landsat observations. Environmental Science and Pollution Research, 29(22), 33152-33166.

[7] Zhang, T., Hu, H., Ma, X., & Zhang, Y. (2020). Long-term spatiotemporal variation and environmental driving forces analyses of algal blooms in Taihu Lake based on multi-source satellite and land observations. Water, 12(4), 1035.

[8] Xue, K., Ma, R., Zhu, G., Hu, M., Cao, Z., Xiong, J., ... & Wu, Y. (2024). A comprehensive time-series dataset linked to cyanobacterial blooms in Lake Taihu. Scientific Data, 11(1), 1365.

[9] Lai, L., Zhang, Y., Han, T., Zhang, M., Cao, Z., Liu, Z., ... & Chen, X. (2024). Satellite mapping reveals phytoplankton biomass's spatio-temporal dynamics and responses to environmental factors in a eutrophic inland lake. Journal of Environmental Management, 360, 121134.

[10] Li, W., Qin, B., & Zhu, G. (2014). Forecasting short-term cyanobacterial blooms in Lake Taihu, China, using a coupled hydrodynamic–algal biomass model. Ecohydrology, 7(2), 794-802.

[11] Wang, J., Wang, Z., Cui, Y., & Yan, S. (2022). Dynamic monitoring of phycocyanin concentration in Chaohu Lake of China using Sentinel-3 images and its indication of cyanobacterial blooms. Ecological Indicators, 143, 109340.

[12] Zhou, T., Li, Y., Jiang, B., Alatalo, J. M., Li, C., & Ni, C. (2023). Tracking spatio-temporal dynamics of harmful algal blooms using long-term MODIS observations of Chaohu Lake in China from 2000 to 2021. Ecological Indicators, 146, 109842.

[13] Liao, Z., Lv, S., Zhang, C., Zha, Y., Wang, S., & Shao, M. (2024). Analysis of Meteorological Drivers of Taihu Lake Algal Blooms over the Past Two Decades and Development of a VOCs Emission Inventory for Algal Bloom. Remote Sensing, 16(10), 1680.

[14] Shi, K., Zhang, Y., Zhou, Y., Liu, X., Zhu, G., Qin, B., & Gao, G. (2017). Long-term MODIS observations of cyanobacterial dynamics in Lake Taihu: Responses to nutrient enrichment and meteorological factors. Scientific reports, 7(1), 40326.

[15] Qin, B., Yang, G., Ma, J., Wu, T., Li, W., Liu, L., ... & Zhou, J. (2018). Spatiotemporal changes of cyanobacterial bloom in large shallow eutrophic Lake Taihu, China. Frontiers in microbiology, 9, 451.

[16] Wang, S., Zhang, X., Wang, C., & Chen, N. (2023). Multivariable integrated risk assessment for cyanobacterial blooms in eutrophic lakes and its spatiotemporal characteristics. Water Research, 228, 119367.

[17] Lin, Q., Zhang, K., McGowan, S., Huang, S., Xue, Q., Capo, E., ... & Shen, J. (2023). Characterization of lacustrine harmful algal blooms using multiple biomarkers: Historical processes, driving synergy, and ecological shifts. Water Research, 235, 119916.

[18] Wang, S., Zhang, X., Chen, N., & Wang, W. (2022). Classifying diurnal changes of cyanobacterial blooms in Lake Taihu to identify hot patterns, seasons and hotspots based on hourly GOCI observations. Journal of environmental management, 310, 114782.

[19] Song, T., Zhang, H., Xu, Y., Dai, X., Fan, F., Wang, Y., & Liu, G. (2024). Cyanobacterial blooms in Lake Taihu: Temporal trends and potential drivers. Science of The Total Environment, 173684.

[20] Yan, L., Xu, Z., Hu, Y., Wang, Y., Zhou, F., Gao, X., ... & Chen, D. (2022). Cyanobacteria bloom hazard function and preliminary application in lake taihu, China. Chemosphere, 307, 136122.

[21] Qiu, Y., Huang, J., Luo, J., Xiao, Q., Shen, M., Xiao, P., ... & Duan, H. (2025). Monitoring, simulation and early warning of cyanobacterial harmful algal blooms: An upgraded framework for eutrophic lakes. Environmental Research, 264, 120296.

[22] Li, J., Liu, Y., Xie, S., Li, M., Chen, L., Wu, C., ... & Luan, Z. (2022). Landsat-satellite-based analysis of long-term temporal spatial dynamics of cyanobacterial blooms: a case study in Taihu Lake. Land, 11(12), 2197.

[23] Wang, S., Zhang, X., Wang, C., & Chen, N. (2023). Temporal continuous monitoring of cyanobacterial blooms in Lake Taihu at an hourly scale using machine learning. Science of the Total Environment, 857, 159480.

[24] Li, S., Liu, C., Sun, P., & Ni, T. (2022). Response of cyanobacterial bloom risk to nitrogen and phosphorus concentrations in large shallow lakes determined through geographical detector: A case study of Taihu Lake, China. Science of The Total Environment, 816, 151617.

[25] Pan, X., Yuan, J., Yang, Z., Tansey, K., Xie, W., Song, H., ... & Yang, Y. (2024). Spatio-Temporal Variation of Cyanobacteria Blooms in Taihu Lake Using Multiple Remote Sensing Indices and Machine Learning. Remote Sensing, 16(5), 889.

[26] Zhang, X., Recknagel, F., Chen, Q., Cao, H., & Li, R. (2015). Spatially-explicit modelling and forecasting of cyanobacteria growth in Lake Taihu by evolutionary computation. Ecological Modelling, 306, 216-225.

[27] Jia, T., Zhang, X., & Dong, R. (2019). Long-term spatial and temporal monitoring of cyanobacteria blooms using MODIS on google earth engine: A case study in Taihu Lake. Remote Sensing, 11(19), 2269.

[28] Li, C., & Wu, W. (2023). Analysis of the driving mechanism of water environment evolution and algal bloom warning signals in tai Lake. Water, 15(6), 1245.

[29] Cao, H., Han, L., & Li, L. (2022). A deep learning method for cyanobacterial harmful algae blooms prediction in Taihu Lake, China. Harmful Algae, 113, 102189.

[30] Shi, K., Zhang, Y., Qin, B., & Zhou, B. (2019). Remote sensing of cyanobacterial blooms in inland waters: present knowledge and future challenges. Science Bulletin, 64(20), 1540-1556.